

Collaborative Active and Reactive Power Optimization for Distribution Networks and Microgrids with Privacy-preserving Feasible Operation Regions Based on Non-iterative Projection Method

Rufeng Zhang, Haodong Liu, Lizhong Lu, Yunjing Liu, Linbo Fu, and Xiaozhuo Guan

Abstract—The integration of numerous distributed energy resources into distribution networks (DNs) can induce large voltage fluctuations and network loss. We introduce a collaborative active and reactive power optimization (CARPO) method for DNs and microgrids (MGs) to efficiently improve the voltage quality and mitigate network loss. First, the CARPO method and models for the DNs and MGs (DMs) are intended to reduce voltage deviations, minimize network loss, and improve the operation efficiency of the entire system. Second, to protect MGs, we aggregate privacy-preserving feasible operation regions of the active and reactive power outputs from distributed energy resources in MGs. A scaled-down MG equivalent model, which ensures high accuracy, is derived for optimal DN operation. Third, based on the equivalent projection theory, the optimal operation flow of DMs with non-iterative projection method is achieved to reduce the computational complexity. The DM model is decomposed into sub-models for the DM levels. The optimal solutions of the coordination variables are obtained for MG power scheduling. Finally, the proposed CARPO method is evaluated through simulation in a modified IEEE 33-bus DN. The results demonstrate that the proposed CARPO method can optimize the system operation and improve the economy of DMs.

Index Terms—Active power, reactive power, distribution network, microgrid, equivalent projection, feasible operation region, network loss.

I. INTRODUCTION

DISTRIBUTED energy resources (DERs) have attracted increasing attention in distribution networks (DNs).

Manuscript received: March 16, 2025; revised: May 12, 2025; accepted: August 20, 2025. Date of CrossCheck: August 20, 2025. Date of online publication: November 25, 2025.

This work was supported by Science and Technology Project Supported by State Grid Corporation of China (No. SGJLJL00XTJS2302012).

This article is distributed under the terms of the Creative Commons Attribution 4.0 International License (<http://creativecommons.org/licenses/by/4.0/>).

R. Zhang, H. Liu, and L. Fu (corresponding author) are with the School of Electrical Engineering, Northeast Electric Power University, Jilin, China (e-mail: zhan-grufeng@necpu.edu.cn; haodong0802@aliyun.com; fulinbo123@aliyun.com).

L. Lu, Y. Liu, and X. Guan are with the State Grid Jilin Power Supply Company, Jilin, China (e-mail: 1696143727@qq.com; 2083645902@qq.com; 1067706632@qq.com).

DOI: 10.35833/MPCE.2025.000221

However, their generation intermittency and volatility cause various problems, including voltage violations [1], [2]. By coordinating the active and reactive power outputs of DERs, the voltage amplitude can be optimized to reduce network loss [3]–[5]. Microgrids (MGs), which are controllable units that integrate DERs and loads, play a key role in the optimal operation of both active and reactive power in DNs, providing flexibility to improve the safety and economy of system operation [6].

Regarding the flexibility quantification of numerous DERs connected to the grid, existing studies have emphasized that the aggregation of flexible resources should not only fully consider the flexibility of DERs but also meet the requirements of privacy protection and efficient solutions while efficiently managing a large number of small-capacity DERs [7], [8]. Computational aggregation flexibility is used to calculate either the Minkowski sum of multiple high-dimensional polytopes or feasible region (FR) projection in a high-dimensional space. In [9], feasible power-injection trajectories at a substation are described using an ellipsoidal inner approximation to efficiently leverage the DER flexibility potential. By modeling and quantifying the aggregate power-injection capacity of DERs in substations within an unbalanced DN, the coordination between the transmission networks and DNs is demonstrated in [10]. In [11], a flexible scheduling interval of aggregators with a robust operation area is integrated to maximize the DER participation in the market while maintaining the DN safety. In [12], power plants are considered to manage numerous DERs for their collective participation in the system operation and electricity markets. In [13], an AC/DC active DN is investigated to aggregate flexibility and serve as a flexible resource in transmission network scheduling. Additionally, a framework for tracking, ranking, and evaluating the flexibility of aggregated DERs in DNs is proposed in [14] by combining an exact alternating optimal power flow model with a cooperative game formula. The aforementioned studies primarily focus on power system flexibility aggregation within a DN. However, with the widespread integration of DERs into MGs, further research is required to explore their flexibility and adaptability.

Solution methods are important to coordinately optimize the operation problem of multiple entities in power grids. Based on the centralized optimization, an auxiliary service market framework for stimulating MGs is proposed in [15] to provide reactive power support to DNs. In [16], a coordinated control strategy is proposed for a multi-MG active DN using encryption to ensure data privacy and integrity. However, these methods generally require global information collection, posing major computational and communication challenges. Several distributed methods have been explored to address this issue. Remarkably, the alternating direction method of multipliers (ADMM) has been widely applied to optimize the power flow of multi-MG and distribution systems [17] and the operation at multiple time scales [18]. As an alternative to ADMM, autonomous DN optimization with multiple MGs based on analytical target cascading is proposed in [19] and decouples DN and MG (DM) optimization scheduling. Furthermore, an improved generalized Benders decomposition for coordinated dynamic economic dispatch in multi-area interconnected systems is proposed in [20]. In

addition, cooperative game theory is applied to the coordinated optimal scheduling of power grids. In [21], a fully coordinated mechanism is introduced for distributed energy trading across interconnected MGs. In [22], the coordinated operation of multi-grid-connected MGs is addressed at the distribution-system level. The consensus method allows to achieve the economic operation of any multi-MG system and relies on MGs that share important global information with other MG controllers [23]. Based on the cutting plane consensus method, the distributed coordination optimization of multi-area dynamic economic dispatch in large-scale power systems is achieved in [24]. Existing centralized methods cannot properly handle large-scale data and related computations, being unsuitable for real-time dynamic scenarios, whereas distributed methods require repeated iterations to achieve a consistent multi-entity optimal strategy, showing demanding communication requirements and poor convergence. Table I provides a comparison of the aforementioned studies on solving methods for multi-entity coordinated optimization.

TABLE I
COMPARISON OF SOLUTION METHODS FOR MULTI-ENTITY COORDINATED OPTIMIZATION

Reference	Method	Research subject	Decomposed	Privacy-preserving	Non-iterative	Computational complexity
[15]	Centralized optimization	DM			✓	High
[16]	Encrypted method	DM		✓	✓	High
[17], [18]	ADMM	DM	✓	✓		Medium
[19]	Analytical target cascading	DM	✓	✓		Medium
[20]	Benders decomposition	Multi-area inter-connected system	✓	✓		High
[21], [22]	Cooperative game	DM	✓	✓		High
[23], [24]	Consensus method	Multi-area inter-connected system	✓	✓		Low
This paper	Equivalent projection (EP)	Multi-level system	✓	✓	✓	Low

Considering existing knowledge gaps, we propose a collaborative active and reactive power optimization (CARPO) method for DM using EP [25] to ensure that the system voltages remain within safe operation limits and privacy preservation in MGs. Compared with existing research, the main contributions of our study are as follows.

1) A coordinated optimization operation framework is proposed that applies CARPO to MGs to enhance the voltage quality in DNs.

2) A generic model of the feasible operation region (FOR) for each MG is established, which describes the power and energy bounds of an MG and ensures privacy preservation for internal DERs.

3) Each MG submits an EP model instead of the original model to participate in optimal DN operation, thereby avoiding iterative processes. This non-iterative projection method avoids computational loops, thereby allowing for an efficient resolution of the DM optimization model via one-round information interaction.

The remainder of this paper is organized as follows. Section II presents the coordinated optimization operation framework for DM. Section III presents the CARPO model of DM and FOR model for MG. In Section IV, we present the non-iterative projection model based on EP. Section V pres-

ents the CARPO model for non-iterative projection calculation of DM. Section VI presents the case study. Finally, Section VII concludes this paper.

II. COORDINATED OPTIMIZATION OPERATION FRAMEWORK FOR DM

The coordinated optimization operation framework for DM comprises the hierarchical DM levels, as shown in Fig. 1.

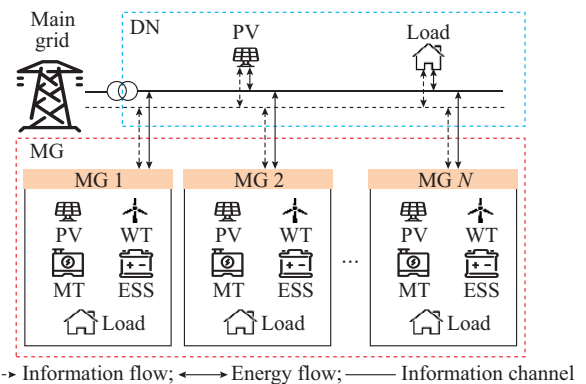


Fig. 1. Coordinated optimization operation framework for DM.

The DN level includes distributed photovoltaic (PV) systems and loads, whereas the MG level includes PV systems, wind turbines (WTs), microturbines (MTs), energy storage systems (ESSs), and loads.

This framework establishes an independent information interaction channel between the systems. The DN collects the PV output predictions, load demands, and FORs from MGs. Using these data, the DN implements a coordinated optimization operation strategy and transmits the outcome to MGs, thereby facilitating a collaborative optimal operation between the two levels.

In terms of energy transfer, the DN optimizes voltage quality, minimizes network loss, and enhances system economy by adjusting the active and reactive power outputs of each source. The DN receives power from the connected distributed PV systems and main grid, as well as additional power support from MG to stabilize any power fluctuations. By adjusting the output of its DERs and charging/discharging strategy of its ESSs, MG improves the operation flexibility and engages in two-way power interactions with the DN to support reliable operation of the entire system. The DERs in an MG not only provide active power support to the DN but also comply with capacity constraints. The reactive power output is regulated by either the inverter (in PV systems and ESSs) or changing the excitation current (in MTs and WTs) to provide reactive power support for the DN, which is important for maintaining the voltage stability and reactive power balance across the grid.

III. CARPO MODEL FOR DM AND FOR MODEL FOR MG

A. CARPO Model for DM

1) Objective Function

The CARPO model for DM minimizes the sum of the DN network loss and DM operation costs. The objective function is expressed as:

$$\min F = \omega_1 \zeta f_1 + \omega_2 (c_2 + c_3) \quad (1)$$

where ζ is a correction coefficient greater than 0, ensuring that all costs in the objective function are in the same order of magnitude; c_2 is the operation cost of DN; c_3 is the operation cost of MG; and ω_1 and ω_2 are the minimal weights satisfying $\omega_1 + \omega_2 = 1$, each of which is greater than 0.

1) Network loss of DN

$$f_1 = \sum_{t=1}^T \sum_{i \in DN} \sum_{j \in v(i)} l_{ij,t} r_{ij} \quad (2)$$

where DN_{bus} is the bus set of DN; T is the optimal operation cycle of the system, which is 24 hours in this paper, and t represents a specific time point in this cycle; $v(i)$ is the set of all end buses, with bus i indicating the initial bus; $l_{ij,t}$ is the square of the current flowing through branch ij at time t ; and r_{ij} is the resistance of branch ij .

2) Operation cost of DN

$$c_2 = \sum_{t=1}^T \sum_{n=1}^N C_{T,t} P_{TDj,t} \quad (3)$$

where $C_{T,t}$ is the time-of-use electricity price of the main grid; $P_{TDj,t}$ is the amount of electricity purchased from the

main grid at DN bus j ; n is the MG index; and N is the set of MGs.

3) Operation cost of MG

$$c_3 = \sum_{t=1}^T \left(\sum_{n=1}^N C_{D,t} P_{DMj,t} + \sum_{n=1}^N C_{MT} P_{MTj,t} + \sum_{n=1}^N C_{ESS} |P_{ESSj,t}| \right) \quad (4)$$

where $C_{D,t}$ is the time-of-use electricity price of DN; $P_{DMj,t}$ is the power purchased from the DN by MG at bus j of the connected DN; C_{MT} is the power generation cost of MT; $P_{MTj,t}$ is the active power output of MT in MG connected to DN bus j ; C_{ESS} is the operation cost of ESS for charging and discharging; and $P_{ESSj,t}$ is the charging and discharging power of ESS in MG connected to DN bus j .

2) DN Operation Constraints

1) Power flow constraints

The DN current model is based on a widely used branch flow model. The corresponding current- and voltage-drop constraints for the model are given by (5) and (6), respectively.

$$\left\| \begin{bmatrix} 2P_{ij,t} & 2Q_{ij,t} & l_{ij,t} - v_{i,t} \end{bmatrix}^T \right\| \leq l_{ij,t} + v_{i,t} \quad (5)$$

$$v_{j,t} = v_{i,t} - 2(r_{ij} P_{ij,t} + x_{ij} Q_{ij,t}) + (r_{ij}^2 + x_{ij}^2) l_{ij,t} \quad (6)$$

where $P_{ij,t}$ and $Q_{ij,t}$ are the active and reactive power flows through branch ij , respectively; $v_{i,t}$ and $v_{j,t}$ are the squares of the voltage amplitudes of buses i and j , respectively; and x_{ij} is the reactance of branch ij .

2) Bus power balance constraints

The power balance at each bus is expressed as:

$$\sum_{i \in u(j)} (P_{ij,t} - l_{ij,t} r_{ij}) + P_{TDj,t} + P_{PVj,t} = \sum_{k \in v(j)} P_{jk,t} + P_{DLj,t} + P_{DMj,t} \quad (7)$$

$$\sum_{i \in u(j)} (Q_{ij,t} - l_{ij,t} x_{ij}) + Q_{TDj,t} + Q_{PVj,t} = \sum_{k \in v(j)} Q_{jk,t} + Q_{DLj,t} + Q_{DMj,t} \quad (8)$$

where $u(j)$ is the set of all initial buses with j indicating the terminal bus; $v(j)$ is the set of all end buses with j indicating the initial bus; $P_{jk,t}$ and $Q_{jk,t}$ are the active and reactive power flows through branch jk , respectively; $Q_{TDj,t}$ is the reactive power injected by bus j from the main grid; $P_{PVj,t}$ and $Q_{PVj,t}$ are the active and reactive power injected by the PV inverter at bus j , respectively; $P_{DLj,t}$ and $Q_{DLj,t}$ are the active and reactive loads at bus j , respectively; and $Q_{DMj,t}$ is the reactive power injected by the DN into MG connected to bus j .

3) Safe-operation constraints

The safe-operation constraints ensure that the voltage and current remain within acceptable limits. In particular, the bus voltage and branch current must satisfy the following conditions:

$$v_i^{\min} \leq v_{i,t} \leq v_i^{\max} \quad (9)$$

$$l_{ij,t} \leq l_{ij}^{\max} \quad (10)$$

where v_i^{\max} and v_i^{\min} are the maximum and minimum squared voltages at bus i , respectively; and l_{ij}^{\max} is the square of the maximum current allowed to flow through branch ij .

4) Control constraints for distributed PV inverter

We adopt the optimal control model for the PV inverters described in [26]. This model allows to adjust both the active and reactive power outputs of the PV inverters. The control constraints are expressed as:

$$\begin{cases} 0 \leq P_{PVj,t} \leq P_{PVj,\max} \\ P_{PVj,t}^2 + Q_{PVj,t}^2 \leq S_{PVj}^2 \\ -P_{PVj,t} \sqrt{1-k_f^2}/k_f \leq Q_{PVj,t} \leq P_{PVj,t} \sqrt{1-k_f^2}/k_f \end{cases} \quad (11)$$

where $P_{PVj,\max}$ is the upper bound of the active power at PV injection bus j ; S_{PVj} is the rated capacity of the distributed PV inverter at bus j ; and $k_f = \cos \theta$ is the minimum power factor of the PV inverter (typically constant).

3) Operation Constraints of MG

1) Active and reactive power output constraints of WT

$$\begin{cases} 0 \leq P_{WTj,t}^M \leq P_{WTj,\max}^M \\ Q_{WTj,\min}^M \leq Q_{WTj,t}^M \leq Q_{WTj,\max}^M \end{cases} \quad (12)$$

where $P_{WTj,t}^M$ and $Q_{WTj,t}^M$ are the active and reactive power outputs from the WT in MG connected to DN bus j , respectively; $P_{WTj,\max}^M$ is the upper bound of the active power output of the WT in MG connected to DN bus j ; and $Q_{WTj,\max}^M$ and $Q_{WTj,\min}^M$ are the upper and lower bounds of the reactive power output of the WT in MG connected to DN bus j , respectively.

2) Active and reactive power output constraints of PV system

$$\begin{cases} 0 \leq P_{PVj,t}^M \leq P_{PVj,\max}^M \\ \left(P_{PVj,t}^M \right)^2 + \left(Q_{PVj,t}^M \right)^2 \leq \left(S_{PVj}^M \right)^2 \\ -P_{PVj,t}^M \sqrt{1-k_f^2}/k_f \leq Q_{PVj,t}^M \leq P_{PVj,t}^M \sqrt{1-k_f^2}/k_f \end{cases} \quad (13)$$

where $P_{PVj,t}^M$ and $Q_{PVj,t}^M$ are the active and reactive power injected into DN bus j by the PV system in MG, respectively; S_{PVj}^M is the rated capacity of PV in MG connected to DN bus j ; and $P_{PVj,\max}^M$ is the upper bound of the active power injected into DN bus j by the PV system in MG.

3) Active and reactive power output constraints of MT

$$\begin{cases} P_{MTj,\min}^M \leq P_{MTj,t}^M \leq P_{MTj,\max}^M \\ \left(P_{MTj,t}^M \right)^2 + \left(Q_{MTj,t}^M \right)^2 \leq \left(S_{MTj}^M \right)^2 \end{cases} \quad (14)$$

where $P_{MTj,t}^M$ and $Q_{MTj,t}^M$ are the active and reactive power outputs injected into DN bus j by MT in MG, respectively; $P_{MTj,\max}^M$ and $P_{MTj,\min}^M$ are the upper and lower bounds of the active power injected into DN bus j by MT in MG, respectively; and S_{MTj}^M is the rated capacity of MT in MG connected to DN bus j .

4) Active and reactive power output constraints of ESS

$$\begin{cases} -P_{ESSj,\max}^M \leq P_{ESSj,t}^M \leq P_{ESSj,\max}^M \\ \left(P_{ESSj,t}^M \right)^2 + \left(Q_{ESSj,t}^M \right)^2 \leq \left(S_{ESSj}^M \right)^2 \\ E_{ESSj,t+1}^M = E_{ESSj,t}^M + P_{ESSj,t}^M \Delta t \\ E_{ESSj,\max}^M \times 10\% \leq E_{ESSj,t}^M \leq E_{ESSj,\max}^M \times 90\% \\ E_{ESSj,0}^M = E_{ESSn,T}^M \end{cases} \quad (15)$$

where $-P_{ESSj,\max}^M$ and $P_{ESSj,\max}^M$ are the upper bounds of active power for charging and discharging ESS in MG connected to DN bus j , respectively; $P_{ESSj,t}^M$ and $Q_{ESSj,t}^M$ are the active and reactive power outputs injected by ESS of MG connected to DN bus j , respectively; S_{ESSj}^M is the apparent power of ESS connected to DN bus j ; and $E_{ESSj,t}^M$ and $E_{ESSj,\max}^M$ are the amounts of electricity and upper energy bound stored in ESS of MG connected to DN bus j , respectively. In general, $E_{ESSj,t}^M$ is set between 10% and 90% of $E_{ESSj,\max}^M$ to protect the battery life. In addition, $E_{ESSj,0}^M$ and $E_{ESSj,T}^M$ are the initial and final values of ESS storage capacity in MG at access bus j during the scheduling period, respectively. The two values are equal and determined by the state of charge of the ESS.

5) MG power balance constraints

$$P_{WTj,t}^M + P_{PVj,t}^M + P_{MTj,t}^M + P_{ESSj,t}^M + P_{DMj,t}^M - P_{MLj,t}^M = 0 \quad (16)$$

$$Q_{WTj,t}^M + Q_{PVj,t}^M + Q_{MTj,t}^M + Q_{ESSj,t}^M + Q_{DMj,t}^M - Q_{MLj,t}^M = 0 \quad (17)$$

where $P_{MLj,t}^M$ and $Q_{MLj,t}^M$ are the active and reactive loads in MG connected to DN bus j , respectively.

B. FOR Model for MG

As independent operations at various power grid levels and the privacy of user data should be guaranteed, DNs face important challenges in collecting global information for optimal scheduling. To address these challenges, the active and reactive power outputs of DERs in an MG should be aggregated, and a privacy-preserving equivalent model that reduces the system complexity while maintaining accuracy for optimal DN operation should be developed.

1) FR Model for Individual DER

The fundamental quantities required to model the active and reactive power outputs of DERs include the maximum and minimum power outputs and energy demand over time. The power and energy boundary model [27] for the FR of an individual DER is adopted as:

$$\underline{p}_{g,t} \leq p_{g,t} \leq \bar{p}_{g,t} \quad (18)$$

$$\underline{e}_{g,t} \leq \sum_{\tau=1}^t p_{g,\tau} \Delta T \leq \bar{e}_{g,t} \quad (19)$$

where subscript g denotes the index of DERs in MG; $\bar{p}_{g,t}$ and $\underline{p}_{g,t}$ are the upper and lower power bounds of DER g , respectively; $\bar{e}_{g,t}$ and $\underline{e}_{g,t}$ are the upper and lower energy bounds of DER g , respectively; τ is the index ranging from 1 to time t ; and ΔT is the minimum operation time in the optimized operating cycle, which is one hour in this paper.

In an MG, DERs can be classified into two categories based on their characteristics. The first category includes DERs that are unconstrained to the input and output energies and unlimited to the time continuity of the power output. These are called generator flexible resources that include PV systems, WTs, and MTs. The second category includes DERs with constraints on both the input and output energies and limited to the time continuity of the power output. These are classified as flexible ESSs. Therefore, $\bar{e}_{g,t}$ and $\underline{e}_{g,t}$ will be divided into two categories $\bar{e}_{gen,t}$, $\bar{e}_{ess,t}$ and $\underline{e}_{gen,t}$, $\underline{e}_{ess,t}$ for calculation, where $\bar{e}_{ess,t}$ and $\underline{e}_{ess,t}$ are the upper and lower

energy bounds of the ESS, respectively; and $\bar{e}_{gen,t}$ and $\underline{e}_{gen,t}$ are the upper and lower energy bounds of the generator. The power and energy boundary model for generator flexible resources is described as:

$$\begin{cases} \bar{e}_{gen,t} = \sum_{\tau=1}^t \bar{p}_{gen,\tau} \\ \underline{e}_{gen,t} = \sum_{\tau=1}^t p_{gen,\tau} \end{cases} \quad (20)$$

where $\bar{p}_{gen,\tau}$ and $p_{gen,\tau}$ are the upper and lower power bounds of the generator, respectively. For flexible ESSs, the upper and lower energy bounds are derived as:

$$\bar{e}_{ess,t}^1 = \min\left(\left(E_{ess,0} + \bar{P}_{ess,t} t \Delta T\right), 90\% E_{ess,max}\right) \quad (21a)$$

$$\bar{e}_{ess,t}^2 = \min\left(\left(E_{ess,0} + P_{ess,t} (T-t) \Delta T\right), 90\% E_{ess,max}\right) \quad (21b)$$

$$\bar{e}_{ess,t} = \min\left(\bar{e}_{ess,t}^1, \bar{e}_{ess,t}^2\right) \quad (21c)$$

$$\underline{e}_{ess,t}^1 = \max\left(\left(E_{ess,0} + P_{ess,t} t \Delta T\right), 10\% E_{ess,max}\right) \quad (22a)$$

$$\underline{e}_{ess,t}^2 = \max\left(\left(E_{ess,0} + \bar{P}_{ess,t} (T-t) \Delta T\right), 10\% E_{ess,max}\right) \quad (22b)$$

$$\underline{e}_{ess,t} = \max\left(\underline{e}_{ess,t}^1, \underline{e}_{ess,t}^2\right) \quad (22c)$$

where $E_{ess,0}$ is the initial state of charge of ESS; $E_{ess,max}$ is the upper energy bound stored in ESSs; and $\bar{p}_{ess,\tau}$ and $p_{ess,\tau}$ are the upper and lower power bounds of ESS, respectively. Note that (21a) and (21b) represent the upper energy bounds pushed backward from the starting time and forward from the ending time, respectively. Next, (21c) indicates that a small value of the upper energy bound described by (21a) and (21b) is the upper energy bound of ESS. The prescribed upper and lower energy bounds are 90% of $E_{ess,max}$ and 10% of $E_{ess,max}$, respectively. The derivation of the lower energy bound is analogous to that of the upper energy bound.

2) Exact FOR Model for MG

The active and reactive power outputs of an MG constitute a polytope obtained by calculating the Minkowski sums of the corresponding FR across all DERs. The exact FOR model of an MG can be expressed as:

$$E_t = \bigcup_{g=1}^G e_{g,t} \quad (23)$$

where \cup denotes the Minkowski sum; G is the number of DERs in MG; $e_{g,t}$ is the upper or lower bound of DER g ; and E_t is the upper or lower energy bound of MG.

Based on [28], the accurate FOR of MG can be determined by calculating the Minkowski sum of FR across all DERs in an MG. Specifically, the Minkowski sum of (20)-(22) is calculated using (23). The sum can be transformed into a projection problem of FOR and calculated using Fourier-Motzkin elimination. Therefore, it is necessary to systematically derive all the constraints generated in the Fourier-Motzkin elimination process and accurately identify the redundant constraints, so that only the non-redundant constraints are retained. The above complex process has been strictly derived and proven in [28].

Overall, the key to eliminating $e_{g,t}$ is to analyze the redundancy of constraints and simplify the operation of the minimum and maximum values, as well as the expression by recombining variables to achieve elimination. The final FOR model constrained by the upper and lower bounds is given by:

$$m_l \leq \mathbf{a}_l^\top \mathbf{E} \leq M_l \quad \forall l \in L \quad (24)$$

where M_l and m_l are the upper and lower boundaries of the exact FOR model, respectively; $\mathbf{E} = [E_T, E_{T-1}, \dots, E_1]^\top$ is a vector with the elements arranged in descending order of time; L is the set of all paths of the $(T+1)$ -dimensional complete binary tree; and \mathbf{a}_l is a T -dimensional column vector comprising all node data on path l , excluding the root nodes. Figure 2 shows the development trends of coefficient a_l , where $a_l(k)$ ($k=1, 2, \dots$) is the coefficient value of the node at stage k on path l .

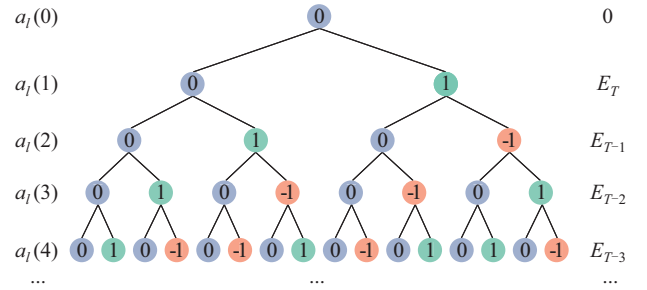


Fig. 2. Development trends of a_l .

For the binary-tree data structure, the root node is assigned with a value of 0. The left child of each node also holds a value of 0, whereas the right child can be assigned either -1 or 1. If a node is the right child of its parent and all ancestor nodes have a value of 0, the value of the node is set to be 1. If any ancestor node has a nonzero value, its value is the opposite to that of the closest nonzero ancestor node. The binary tree is traversed in this manner across all nodes.

Let $b_l(t)$ be defined as:

$$b_l(t) \triangleq \sum_{\tau=1}^t a_l(\tau) \quad \forall t \in [1, T] \quad (25)$$

This leads to the following equivalent expression:

$$\mathbf{b}_l^\top \mathbf{P} \Delta T = \mathbf{a}_l^\top \mathbf{E} \quad (26)$$

where \mathbf{P} is the power vector.

Thus, (24) can be expressed as:

$$m_l \leq \mathbf{b}_l^\top \mathbf{P} \Delta T \leq M_l \quad \forall l \in L \quad (27)$$

Based on the parity of the number of nonzero nodes along the path of the binary tree, the upper and lower bounds of (27) can be determined. When the number of nonzero nodes in the path is odd, the upper and lower bounds are expressed as:

$$M_l \triangleq \sum_{g \in G} \min \left\{ \bar{e}_g(S_l) - \Delta T \left\langle \mathbf{1} - \mathbf{b}_l, \underline{\mathbf{p}}_g \right\rangle_{[s_l; r_l-1]}, \Delta T \left\langle \mathbf{b}_l, \bar{\mathbf{p}}_g \right\rangle_{[s_l; r_l-1]} + \bar{e}_g(R_l) \right\} \quad (28)$$

$$m_l \triangleq \sum_{g \in G} \max \left\{ e_g(S_l) - \Delta T \langle \mathbf{1} - \mathbf{b}_l, \bar{\mathbf{p}}_g \rangle_{[s_l:r_l-1]}, \right. \\ \left. \Delta T \langle \mathbf{b}_l, \underline{\mathbf{p}}_g \rangle_{[s_l:r_l-1]} + e_g(R_l) \right\} \quad (29)$$

where $\langle \mathbf{x}, \mathbf{y} \rangle_{[a:b]} = \langle \mathbf{x} \rangle_{[a:b]}^T \langle \mathbf{y} \rangle_{[a:b]}$; and s_l and r_l are the first and last nonzero element indices on path l , respectively. When the number of nonzero nodes in the path of a binary tree is even, the upper and lower bounds are expressed as:

$$M_l \triangleq \sum_{g \in G} \min \left\{ \bar{e}_g(S_l) - \underline{e}_g(R_l) - \right. \\ \left. \Delta T \langle \mathbf{1} - \mathbf{b}_l, \underline{\mathbf{p}}_g \rangle_{[s_l:r_l-1]}, \Delta T \langle \mathbf{b}_l, \bar{\mathbf{p}}_g \rangle_{[s_l:r_l-1]} \right\} \quad (30)$$

$$m_l \triangleq \sum_{g \in G} \max \left\{ e_g(S_l) - \bar{e}_g(R_l) - \right. \\ \left. \Delta T \langle \mathbf{1} - \mathbf{b}_l, \bar{\mathbf{p}}_g \rangle_{[s_l:r_l-1]}, \Delta T \langle \mathbf{b}_l, \underline{\mathbf{p}}_g \rangle_{[s_l:r_l-1]} \right\} \quad (31)$$

S_l and R_l are defined as:

$$S_l \triangleq T + 1 - s_l \quad (32)$$

$$R_l \triangleq T + 1 - r_l \quad (33)$$

The above expressions show that the number of constraints in the exact FOR model of an MG is independent of the number of aggregated DERs. However, it varies exponentially with the number of layers in the complete binary tree, i. e., the number of divided time periods. The exact FOR model contains $2^T - 1$ valid paths, none of which are zero. Each path corresponds to the upper and lower bounds. Considering both the active and reactive power outputs, the total number of parameters is $4(2^T - 1)$. Under intraday scheduling, T is 24, resulting in 67, 108, and 860 parameters. This level of computational complexity is impractical.

3) FOR Model Under k -order Approximation

We apply a k -order approximation to the exact FOR model, which selects paths based on the number of nonzero nodes along each path. In particular, the k -order approximation involves choosing paths containing no more than k nonzero nodes to form constraints. Thus, the FOR model under the k -order approximation can be expressed as:

$$m_l \leq \mathbf{b}_l^T \mathbf{P} \Delta T \leq M_l \quad \forall l \in L_k, L_k \triangleq \left\{ l \in L \left| \sum_{i=1}^T |a_l(i)| \leq k \right. \right\} \quad (34)$$

where L_k is the set of paths selected by k -order approximation.

As the approximation order increases, the computational accuracy increases, but the complexity also increases.

Since an MG aggregates the active and reactive power FRs of DERs, the upper and lower bounds of MG output are calculated and uploaded to DN for coordinated optimization. Thus, the DN does not collect specific parameters of DER output in MG. Therefore, DM optimization for operation model can be expressed as:

$$\begin{cases} \min F = \omega_1 \zeta f_1 + \omega_2 (c_2 + c_3) \\ \text{s.t. (5)-(11), (34)} \end{cases} \quad (35)$$

IV. NON-ITERATIVE PROJECTION MODEL BASED ON EP

A. Non-iterative Projection Model of DM

In DM, the decision variables are classified into two categories based on their characteristics as coordination variables x such as the interaction power between DN and MGs, and internal variables y such as the output power of DERs in an MG.

The non-iterative projection model for DM can be expressed as:

$$\min_{x,y} F = \omega_1 \zeta f_1 + \omega_2 (c_2 + c_3) \quad (36a)$$

s.t.

$$h^D(x_N, y^D) \leq 0 \quad (36b)$$

$$h_n^M(x_n, y_n^M) \leq 0 \quad \forall n \in N \quad (36c)$$

where $h^D(\cdot)$ and $h_n^M(\cdot)$ are the constraints of DN level and MG n , respectively; x_N is the set of all coordination variables related to all MGs; x_n is the set of all coordination variables related to MG n ; and y^D and y_n^M are the internal variables of DN level and MG n , respectively.

Owing to coordination variable x , DM levels cannot be optimized independently. However, if x is fixed, a hierarchical method can be adopted to solve the joint optimization problem. We use EP to eliminate internal variable y in MG optimization model without altering the system optimality, which characterizes the MG operation using a set of inequality constraints on coordination variable x . The MG operation cost is transformed into an inequality using an epigraph [29] as follows. Let $c_{3,n}$ and C_n be the cost function and operation cost of MG n , respectively. \bar{C}_n is introduced to limit the value of C_n , which can take any value larger than the $c_{3,n}$ supremum. The non-iterative projection model can be modified as:

$$\min_{x,y,C} F = \omega_1 \zeta f_1 + \omega_2 \left(c_2 + \sum_{n \in N} C_n \right) \quad (37a)$$

s.t.

$$h^D(x_N, y^D) \leq 0 \quad (37b)$$

$$h_n^M(x_n, y_n^M) \leq 0 \quad \forall n \in N \quad (37c)$$

$$c_{3,n} \leq C_n \leq \bar{C}_n \quad \forall n \in N \quad (37d)$$

where C is the cost function in the objective function; and C_n is the augmented coordination variable for MG n , and DM is coupled only by (x_n, C_n) . Hence, y_n^M is confined to MG constraints and does not appear in its objective function, thereby protecting sensitive information such as the cost at MG level.

The FOR per MG is defined as a set of variables that satisfy the corresponding operation constraints and can be expressed as:

$$\Theta_n = \left\{ (x_n, C_n, y_n^M) \in \mathbb{R}^{N_x+1} \times \mathbb{R}^{N_y}; (37c), (37d) \right\} \quad (38)$$

where N_x and N_y are the dimensions of x and y , respectively; and Θ_n is a polytope in $\mathbb{R}^{N_x+1} \times \mathbb{R}^{N_y}$ space.

The EP model of FOR of MG n , i.e., in (x_n, C_n) subspace, can be expressed as:

$$\Pi_n = \left\{ (x_n, C_n) \in \mathbb{R}^{N_s+1}; \exists y_n^M, \text{s.t. } (x_n, C_n, y_n^M) \in \Theta_n \right\} \quad (39)$$

Each MG submits its reduced-dimensional EP model, rather than the original model, for coordinated optimization of operation at the DN level. Consequently, the original model in (37) can be decomposed into separate optimization models at DM levels.

The DN-level optimization model is expressed as:

$$\min_{x, y^D, C} F = \omega_1 \zeta f_1 + \omega_2 \left(c_2 + \sum_{n \in N} C_n \right) \quad (40a)$$

s.t.

$$h^D(x_N, y^D) \leq 0 \quad (40b)$$

$$(x_n, C_n) \in \Pi_n \quad \forall n \in N \quad (40c)$$

The MG-level optimization model is expressed as:

$$\min_{y_n^M} c_3 = \sum_{n \in N} c_{3,n} \quad (41a)$$

s.t.

$$h_n^M(\tilde{x}_n, y_n^M) \leq 0 \quad \forall n \in N \quad (41b)$$

$$c_{3,n} \leq \tilde{C}_n \quad \forall n \in N \quad (41c)$$

where \tilde{x}_n and \tilde{C}_n are the optimal solutions for the DN-level optimization model.

B. MG Power Decomposition

The MG-level optimization model uses \tilde{x}_n and \tilde{C}_n as boundary conditions to calculate the optimal values of internal variables y_n^M of MGs, which represent the optimal operation points. The overall output of MG is then decomposed into individual DERs. The MG power decomposition model is expressed as:

$$\begin{cases} \min \delta = \left| y_n^M - \sum_{g=1}^G y_{n,g}^M \right| \\ \text{s.t. (12)-(17), (34), (41b), (41c)} \end{cases} \quad (42)$$

where δ is the decomposition error; and $y_{n,g}^M$ is the specific output of the g^{th} DER in MG n . This model accurately decomposes the total output power of an MG into its constituent DERs.

V. CARPO MODEL FOR NON-ITERATIVE PROJECTION CALCULATION OF DM

A. Theoretical Framework

The CARPO model for DM employs a solution procedure involving both bottom-up aggregation and top-down decomposition. This facilitates the coordinated and optimized operation of DM through a one-round information interaction. The calculation steps are detailed as follows.

1) *Step 1*: form FR of individual DER.

The FR for the active and reactive power outputs of each DER is established considering the model given by (18) and (19). This is achieved by inputting the upper and lower bounds of the active and reactive power outputs per DER.

2) *Step 2*: form FOR model for MG n .

The Minkowski sum of the output FRs from all DERs in

MG is calculated to obtain the model in (27). The FOR model under the k -order approximation model in (34) reduces the computational complexity.

3) *Step 3*: derive EP model of FOR of MG.

By using the EP model in (39) represented in the (x_n, C_n) subspace, y_n^M is eliminated, and the FR of x_n with respect to C_n is obtained.

4) *Step 4*: construct DN-level optimization model considering MG operation constraints.

The EP model in (39) in (x_n, C_n) subspace is adopted as a condition for MG operation, and the DN-level optimization model in (40) is obtained.

5) *Step 5*: solve the model to obtain coordination variable x_n and C_n .

Basic data such as x_n , C_n , x_N , and y^D are input to solve the model in (40). The optimal values of \tilde{x}_n and \tilde{C}_n are obtained.

6) *Step 6*: determine total output of MG n .

\tilde{x}_n and \tilde{C}_n obtained in *Step 5* are used to solve the MG-level optimization model in (41), and the total output of all DERs in MG n is obtained.

7) *Step 7*: derive output power per DER.

By using the MG power decomposition model in (42), the total output of MG is distributed across the individual DERs, and the CARPO results per DER are obtained.

B. Practical Applications

In practice, FRs of DERs are obtained according to the upper and lower bounds of the active and reactive power outputs per DER. Subsequently, FRs of DERs are input into the corresponding FOR model of MGs, and FORs of MGs are obtained and uploaded to DN by MGs. Furthermore, DN performs CARPO and determines the interactive power results between DM, and the active and reactive power dispatch results of DERs in the DN are determined simultaneously. The interactive power results between DM are transmitted to the corresponding MG, and MGs decompose the obtained total output to each DER by minimizing the cost of each MG. This process only involves transmission of power information at the coupling point of the DM and is non-iterative. The CARPO model for DM ensures the privacy and efficiency of DM in practical applications.

VI. CASE STUDY

A. Parameter Settings

We applied a modified IEEE 33-bus DN as a case study to validate the CARPO model for DM. Distributed PV systems were connected at buses 7, 11, 18, 19, 27, and 33 of DN with installation capacities of 1, 1, 2.5, 1, 1.25, and 1.25 MVA, respectively. Furthermore, four MGs were integrated into buses 15, 22, 24, and 31 in DN. Figure 3 illustrates the topology for the modified IEEE 33-bus DN. The DN was operated at a voltage of 12.66 kV with the total active and reactive loads of 3715 kW and 2300 kvar, respectively. The voltage at bus 1 was set to be 1 p.u., and the voltages at the other buses were constrained within the safe operation range of 0.95-1.05 p.u.. ω_1 and ω_2 were both set to be 0.5.

An accurate FOR model for MGs was applied for approxi-

mate calculations using a second-order approximation [30]. Figure 4 shows the daily load and PV output prediction curves in DN, and Fig. 5 shows the daily load profiles of the four MGs.

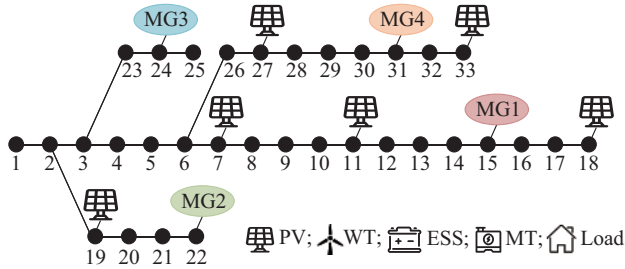


Fig. 3. Topology for modified IEEE 33-bus DN.

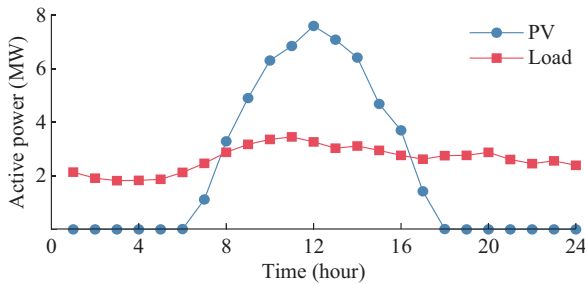


Fig. 4. Daily load and PV output prediction curves in DN.

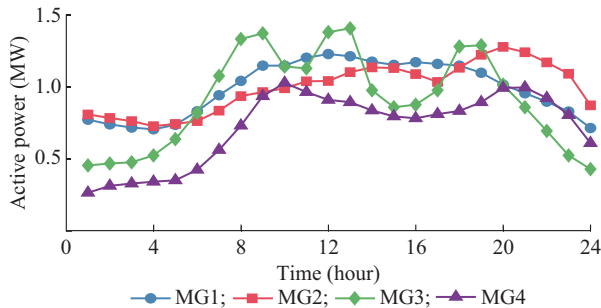


Fig. 5. Daily load profiles of four MGs.

Following [30], we apply a second-order approximation to the exact FOR model of MG. Taking MG4 as an example, we provide the upper and lower bounds of power flexibility under the second-order approximation, as shown in Fig. 6. The space between M_l and m_l defines the power flexibility of MG4. As the flexibility of the DERs accumulates over time, the space between the upper and lower bounds of the power flexibility gradually increases.

B. Comparative Analysis of Optimization Results

To evaluate the effectiveness of the CARPO model for DM, we consider the following three cases.

- 1) Case 1: independent optimal operation of DM.
- 2) Case 2: optimization of collaborative operation of DM using non-iterative projection method without considering reactive power support from MG to DN.
- 3) Case 3: optimization of collaborative operation of DM using non-iterative projection method considering reactive power support from MG to DN.

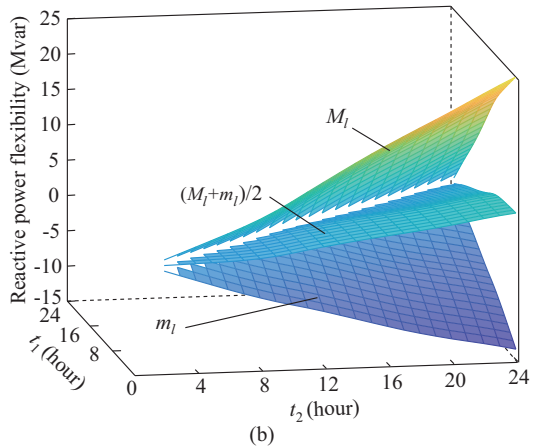
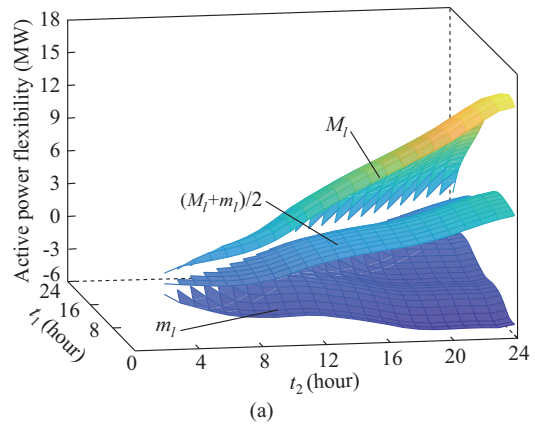


Fig. 6. Upper and lower bounds of power flexibility under second-order approximation. (a) Active power. (b) Reactive power.

1) Voltage Optimization Results of DN

Figure 7 shows the voltage magnitudes for the three cases. In case 1, because of the high output of the PV system, the voltage increases between the 10th hour and the 14th hour. Consequently, some weak buses experience voltages that exceed the upper bound. Notably, at the 12th hour, the voltage at bus 18 reaches a peak of 1.0732 p.u.. However, between the 18th hour and the 24th hour, the high-load level of DN and reduced output from the PV system result in a voltage drop, causing some buses to experience the voltage below the lower bound. At the 20th hour, the lowest voltage at bus 18 is observed at 0.9339 p.u.. The total voltage deviation in DN over 24 hours is 0.6710 p.u.. In case 2, DM maintains separate supply-demand balances for reactive power. Although the voltage at each bus remains within a safe operation range, large voltage fluctuations up to 0.4306 p.u. occur in DN. In case 3, the reactive power generated by DERs in MG initially satisfies the internal reactive power demand of MG. The surplus reactive power is then injected into DN. Consequently, the total voltage deviation in DN decreases to 0.2428 p.u., which is 63.82% and 43.62% lower than those in cases 1 and 2, respectively. These results demonstrate that the CARPO model for DM mitigates the voltage fluctuations in DN, thereby improving the overall voltage quality across the grid.

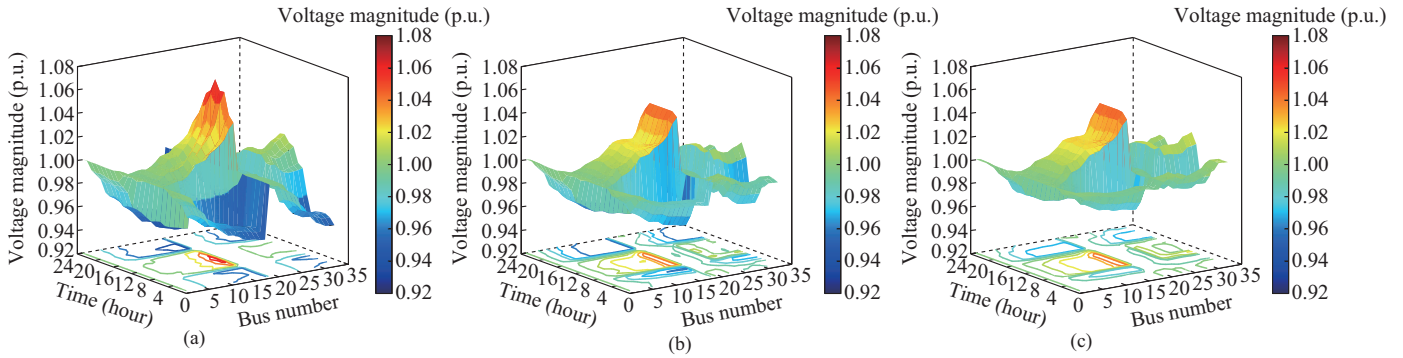


Fig. 7. Voltage magnitudes for three cases. (a) Case 1. (b) Case 2. (c) Case 3.

2) Results of MG Scheduling Strategy

Figure 8 shows the power balance of MG1 in different cases. A positive value indicates that power is injected into MG from DN, whereas a negative value indicates that power flows from MG to DN. In case 1, as shown in Fig. 8(a) and (d), MG operates in islanded mode. The ESS charges when the DER output exceeds the load demand. In contrast, when the DER output does not satisfy the load demand, the ESS discharges to ensure power self-sufficiency. In case 2, active power interactions occur between MG and DN, as shown in Figs. 8(b) and (e). As MG1 is adjacent to bus 18 from the 9th hour to the 15th hour, MG satisfies the minimum active

output constraint of MT, and the remaining power is sourced from the surplus generated by the distributed PV system in DN. During this period, ESS stores the surplus power after satisfying the load demand, and DERs of MG provide reactive power to satisfy the internal reactive power requirements. In case 3, as depicted in Fig. 8(c) and (f), active power scheduling for MG1 is similar to that in case 2, except for the addition of reactive power interactions between MG and DN. Again, MG satisfies its internal reactive power demand and 5.41 Mvar of reactive power is injected into DN, thereby reducing voltage deviations and minimizing network loss.

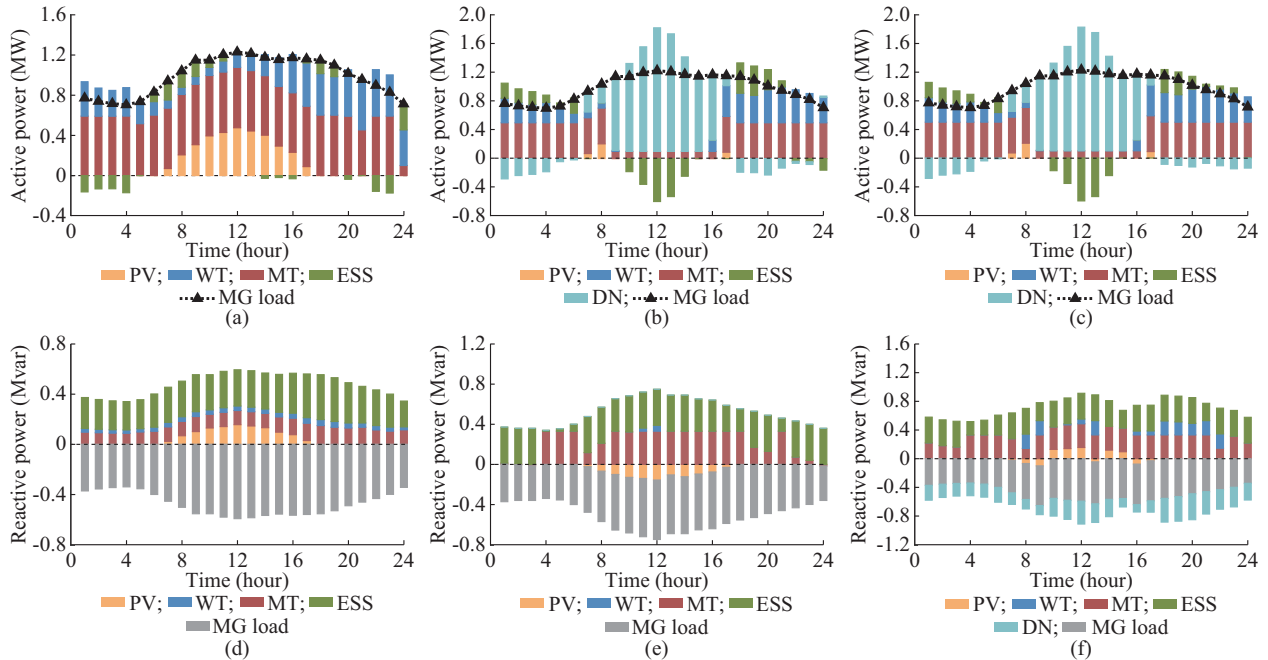


Fig. 8. Power balance of MG1 in different cases. (a) Active power of case 1. (b) Active power of case 2. (c) Active power of case 3. (d) Reactive power of case 1. (e) Reactive power of case 2. (f) Reactive power of case 3.

Figure 9 shows the power balance of MG3 in different cases. As shown in Fig. 9(a) and (d), the scheduling strategy of MG3 in case 1 is similar to that of MG1. The MG supplies power to the load via PV and WT generation. ESS charges when the load demand is low and discharges when the load demand increases. As shown in Fig. 9(b) and (c), the active power of MG3 in cases 2 and 3 is similar, except for slight differences in the ESS charging and discharging

strategies. However, as shown in Fig. 9(e) and (f), compared with case 2, MG3 in case 3 injects additional reactive power of 6.73 Mvar to provide reactive support to DN, further reducing the voltage deviations and network loss in DN. These results demonstrate that the CARPO model for DM optimizes the use of MG resources and minimizes voltage deviations and network loss by optimizing active and reactive power.

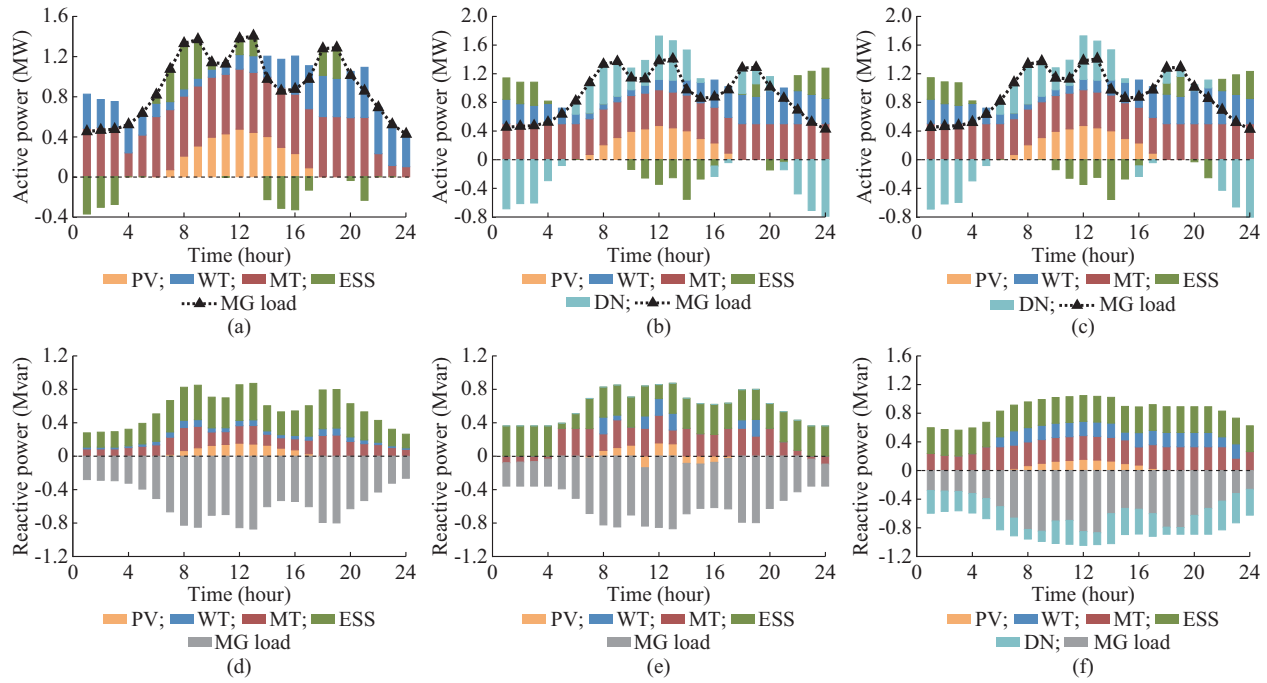


Fig. 9. Power balance of MG3 in different cases. (a) Active power of case 1. (b) Active power of case 2. (c) Active power of case 3. (d) Reactive power of case 1. (e) Reactive power of case 2. (f) Reactive power of case 3.

Figure 10 shows the ESS charging/discharging strategy and time-of-use electricity price in case 3. Between the 0th hour and the 6th hour, the electricity price is relatively high when no PV power is generated. During this period, DN relies on traditional power sources to satisfy its demand. Therefore, the ESS discharges to satisfy the load demand of MG and supplies surplus power to DN. Between the 17th hour and the 24th hour, as PV generation decreases and electricity prices increase, ESS discharges to meet the load demand and supplies surplus power to DN. By the 24th hour, ESS returns to the state of charge at the 0th hour. This charging/discharging strategy mitigates the power fluctuations in DN and enables peak-valley arbitrage through low-price charging and high-price discharging, thereby drastically reducing the operation costs of MG.

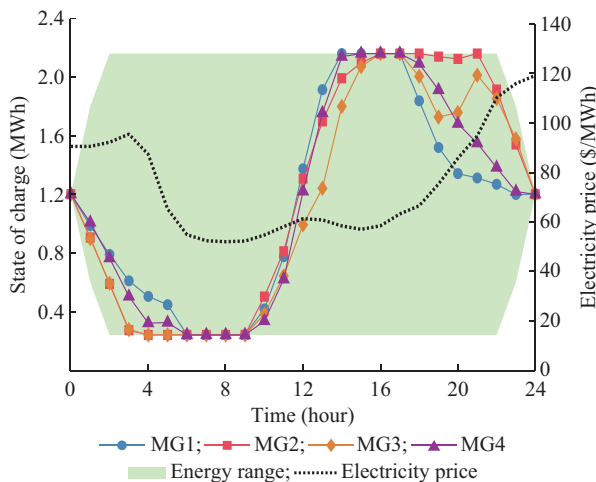


Fig. 10. ESS charging/discharging strategy and time-of-use electricity price in case 3.

3) Operation Cost

Table II lists the operation costs in the three cases. Compared with that of case 1, the cost of purchasing power from the DN is drastically lower in cases 2 and 3 because MG can coordinate with DN. Thus, MGs consume surplus power when the PV output of DN is excessive and can deliver power to DN under insufficient PV output if the load demand of MG is low, thereby reducing the cost of purchasing power from the main grid by DN.

TABLE II
OPERATION COSTS IN THREE CASES

Case	Operation cost of DN (\$)	Operation cost (\$)				
		MG1	MG2	MG3	MG4	Total
Case 1	3756.50	1699.50	1704.85	1588.04	893.68	9642.58
Case 2	2622.76	1671.79	1626.17	1378.90	1157.34	8456.97
Case 3	2583.56	1644.52	1628.34	1395.09	1149.88	8401.39

A slight difference occurs in the operation costs of MG in cases 2 and 3 because the active power output of MG1-MG4 remains unchanged. However, the operation costs of MG4 are higher in cases 2 and 3 than that in case 1. This could be attributed to that MG4 is closer to bus 33 with weak bus voltage. When the PV output at this bus does not satisfy the load demand, the voltage could drop below the acceptable limits. To prevent a voltage sag in DN, MT in MG increases its power output to increase the voltage, which increases the operation costs of MG4.

Although the operation cost in case 3 is only \$55.58 lower than that in case 2, the power output strategy in case 3 outperforms that in case 2 by reducing voltage fluctuations and network loss in DN. In particular, the total cost in case

2 is 12.30% lower than that in case 1, whereas the total cost in case 3 is 12.87% lower than that in case 1. These results indicate that CARPO between DM considerably reduces the operation costs of the overall system.

4) Influence of Weights on Objective Function

According to the objective function in (1), different weights affect the results of the optimal operation of DM. Therefore, we investigate the influence of different weights on the network loss and system costs. Let $\omega_1 + \omega_2 = 1$. Different weights (ω_1, ω_2) are set as: $C_1 = (0.9, 0.1)$, $C_2 = (0.7, 0.3)$, $C_3 = (0.5, 0.5)$, $C_4 = (0.3, 0.7)$, and $C_5 = (0.1, 0.9)$. Table III lists the comparison of network loss and system cost under different weights. With decreasing weights of ω_1 , the network loss increases. With increasing weight of ω_2 , the total cost decreases. Therefore, changing the weights in the CARPO model for DM could balance the minimum degree of network loss and total cost and make the power grid operation more flexible and economical.

TABLE III
COMPARISON OF NETWORK LOSS AND SYSTEM COST UNDER DIFFERENT WEIGHTS

Combination	Network loss (MWh)	DN-level cost (\$)	MG-level cost (\$)	Total cost (\$)
C_1	1.244	3234.26	5475.72	8709.99
C_2	1.313	2940.61	5510.36	8450.97
C_3	1.352	2880.98	5520.42	8401.39
C_4	1.381	2859.63	5529.61	8389.23
C_5	1.396	2855.94	5536.00	8391.94

C. Performance of Approximation Model

1) Decomposition Error

In this study, we use a k -order approximation model instead of an exact FOR model for MG. In Table IV, the decomposition errors of k -order approximation models are listed. The decomposition errors for both active and reactive power are almost negligible for the second-order approximation model, indicating high accuracy. Although the model complexity drastically increases for the third- and fourth-order approximation models, the decomposition errors remain almost unchanged.

TABLE IV
DECOMPOSITION ERRORS OF k -ORDER APPROXIMATION MODELS

Order	Number of L_k	Active power decomposition error (MW)	Reactive power decomposition error (Mvar)
1	24	18.38	3.05
2	300	10^{-10}	10^{-10}
3	2324	10^{-10}	10^{-10}
4	12950	10^{-10}	10^{-10}

2) Computational Time

Figure 11 compares the modeling time and solution time from the first- to fourth-order approximation models. As the approximation order increases, the model complexity also in-

creases, thus increasing the modeling time. However, this change remains relatively stable over time. Similarly, the solution time increases with the approximation order, and the solution complexity increases rapidly at higher approximation orders. Nevertheless, the modeling complexity and solution time from the first- to fourth-order approximation models are acceptable, indicating that the scale and complexity of the approximation model do not impose excessive computational burden.

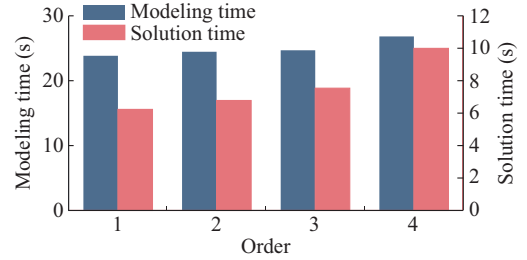


Fig. 11. Modeling time and solution time from first- to fourth-order approximation models.

Overall, considering the decomposition error and computational time, the second-order approximation model exhibits a suitable balance between accuracy and computational complexity, being the most appropriate approximation for the exact FOR model of an MG.

3) Error Analysis

Table V lists the errors in optimization objectives including voltage deviation, network loss, and total cost according to the approximation order. The values of the objective function from the second- to fourth-order approximations are the same, corresponding to the minimum errors in Table IV, and the accuracy of the second- and higher-order approximations is confirmed. The voltage deviation, network loss, and total cost errors of the first-order approximation relative to the higher-order approximation are 21.03%, 7.43%, and 39.67%, respectively, further demonstrating the inaccuracy of the calculation results for the first-order approximation.

TABLE V
ERRORS IN OPTIMIZATION OBJECTIVES INCLUDING VOLTAGE DEVIATION, NETWORK LOSS, AND TOTAL COST ACCORDING TO APPROXIMATION ORDER

Order	Voltage deviation error (p.u.)	Network loss error (MWh)	Total cost error (\$)
1	0.1917	1.2511	5068.84
2	0.2428	1.3515	8401.39
3	0.2428	1.3515	8401.39
4	0.2428	1.3515	8401.39

VII. CONCLUSION

To address persistent voltage violation and network loss in DNs owing to the high integration of DERs, we aggregate the active and reactive power outputs of DERs using the FOR model for optimization. Considering the strong coupling between the active and reactive power outputs in both DM, the CARPO method for DM is formulated to optimize the system operation. The proposed CARPO method can be

solved using non-iterative projection method based on EP. The proposed CARPO method is validated through simulations using a modified IEEE 33-bus distribution system. The following conclusions can be drawn from the results.

1) MG aggregates DERs to form an exact FOR model, safeguarding the internal MG parameters and related private information. A k -order approximation model accurately approximates the exact FOR model. By using the second-order approximation, the number of parameters is reduced from 67, 108, 860 to 1200, with the decomposition error limited to 10^{-10} . This reduction in the number of parameters leads to the decrease in the computational complexity while maintaining the calculation accuracy.

2) Compared with the independent operation of each power grid, the economy and stability of the system operation can be improved by considering active power interactions in DM. The voltage deviation in DN and the system operation cost are reduced by 63.82% and 12.87%, respectively, while the network loss also decreases. This greatly improves the security and economy of the system.

3) Non-iterative projection maps FOR of MG onto the boundary of DN. The resulting privacy-preserving equivalent model of MG is incorporated into the optimal DN operation. Through a one-round information interaction, the decision outcomes of the DN align with the optimal solutions at the MG level, thereby facilitating the efficient coordination optimization of both systems.

In this study, the influence of uncertainty caused by the intermittency and randomness of the DER is not considered. In the future, we will address the influence of uncertainty factors on the coordinated optimization operation strategy of MGs.

REFERENCES

- [1] Q. Ma and C. Deng, "Deterministic and robust volt-var control methods of power system based on convex deep learning," *Journal of Modern Power Systems and Clean Energy*, vol. 12, no. 3, pp. 719-729, May 2024.
- [2] Y. Zhang, K. Lin, W. Deng *et al.*, "A flexible voltage control strategy based on stage-division for microgrids," *Protection and Control of Modern Power Systems*, vol. 9, no. 3, pp. 60-69, May 2024.
- [3] S. Chen, C. Wang, and Z. Zhang, "Multi-time scale active and reactive power coordinated optimal dispatch in active distribution network considering multiple correlation of renewable energy sources," *IEEE Transactions on Industry Applications*, vol. 57, no. 6, pp. 5614-5625, Nov. 2021.
- [4] J. Xu, H. Gao, R. Wang *et al.*, "Real-time operation optimization in active distribution networks based on multi-agent deep reinforcement learning," *Journal of Modern Power Systems and Clean Energy*, vol. 12, no. 3, pp. 886-899, May 2024.
- [5] Z. Huang, Y. Zhang, and S. Xie, "Data-adaptive robust coordinated optimization of dynamic active and reactive power flow in active distribution networks," *Renewable Energy*, vol. 188, pp. 164-183, Apr. 2022.
- [6] M. Zhang, Y. Han, Y. Liu *et al.*, "Multi-time scale modeling and dynamic stability analysis for sustainable microgrids: state-of-the-art and perspectives," *Protection and Control of Modern Power Systems*, vol. 9, no. 3, pp. 1-35, May 2024.
- [7] J. Bendtsen, K. Trangbaek, and J. Stoustrup, "Hierarchical model predictive control for resource distribution," in *Proceedings of 49th IEEE Conference on Decision and Control*, Atlanta, USA, Dec. 2010, pp. 2468-2473.
- [8] H. Hao, B. M. Sanandaji, K. Poolla *et al.*, "Aggregate flexibility of thermostatically controlled loads," *IEEE Transactions on Power Systems*, vol. 30, no. 1, pp. 189-198, Jan. 2015.
- [9] B. Cui, A. Zamzam, and A. Bernstein, "Network-cognizant time-coupled aggregate flexibility of distribution systems under uncertainties," *IEEE Control Systems Letters*, vol. 5, no. 5, pp. 1723-1728, Nov. 2021.
- [10] X. Chen, E. Dall'Anese, C. Zhao *et al.*, "Aggregate power flexibility in unbalanced distribution systems," *IEEE Transactions on Smart Grid*, vol. 11, no. 1, pp. 258-269, Jan. 2020.
- [11] J. S. Russell, P. Scott, and J. Iria, "Network-secure aggregator operating regions with flexible dispatch envelopes in unbalanced systems," *Electric Power Systems Research*, vol. 235, p. 110728, Oct. 2024.
- [12] S. Wang and W. Wu, "Aggregate flexibility of virtual power plants with temporal coupling constraints," *IEEE Transactions on Smart Grid*, vol. 12, no. 6, pp. 5043-5051, Nov. 2021.
- [13] X. Huang, P. Dong, X. He *et al.*, "Research on aggregation flexibility method of AC/DC distribution network considering flexibility balance and its application," *IEEE Systems Journal*, vol. 17, no. 3, pp. 3635-3645, Sept. 2023.
- [14] A. Churkin, W. Kong, J. N. M. Gutierrez *et al.*, "Tracing, ranking and valuation of aggregated DER flexibility in active distribution networks," *IEEE Transactions on Smart Grid*, vol. 15, no. 2, pp. 1694-1711, Mar. 2023.
- [15] A. G. Madureira and J. A. P. Lopes, "Ancillary services market framework for voltage control in distribution networks with microgrids," *Electric Power Systems Research*, vol. 86, pp. 1-7, May 2012.
- [16] X. Sun, J. Qiu, Y. Ma *et al.*, "Encryption-based coordinated volt/var control for distribution networks with multi-microgrids," *IEEE Transactions on Power Systems*, vol. 38, no. 6, pp. 5909-5921, Nov. 2023.
- [17] C. Tang, M. Liu, Y. Dai *et al.*, "Decentralized saddle-point dynamics solution for optimal power flow of distribution systems with multi-microgrids," *Applied Energy*, vol. 252, p. 113361, Oct. 2019.
- [18] L. Chen, X. Zhu, J. Cai *et al.*, "Multi-time scale coordinated optimal dispatch of microgrid cluster based on MAS," *Electric Power Systems Research*, vol. 177, p. 105976, Dec. 2019.
- [19] M. Xie, X. Ji, X. Hu *et al.*, "Autonomous optimized economic dispatch of active distribution system with multi-microgrids," *Energy*, vol. 153, pp. 479-489, Jun. 2018.
- [20] Z. Li, W. Wu, B. Zhang *et al.*, "Decentralized multi-area dynamic economic dispatch using modified generalized benders decomposition," *IEEE Transactions on Power Systems*, vol. 31, no. 1, pp. 526-538, Jan. 2016.
- [21] J. Lee, J. Guo, J. K. Choi *et al.*, "Distributed energy trading in microgrids: a game-theoretic model and its equilibrium analysis," *IEEE Transactions on Industrial Electronics*, vol. 62, no. 6, pp. 3524-3533, Jun. 2015.
- [22] Y. Du, Z. Wang, G. Liu *et al.*, "A cooperative game approach for coordinating multi-microgrid operation within distribution systems," *Applied Energy*, vol. 222, pp. 383-395, Jul. 2018.
- [23] M. N. Alam, S. Chakrabarti, and A. Ghosh, "Networked microgrids: state-of-the-art and future perspectives," *IEEE Transactions on Industrial Informatics*, vol. 15, no. 3, pp. 1238-1250, Mar. 2019.
- [24] W. Zhao, M. Liu, J. Zhu *et al.*, "Fully decentralised multi-area dynamic economic dispatch for large-scale power systems via cutting plane consensus," *IET Generation, Transmission & Distribution*, vol. 10, no. 10, pp. 2486-2495, Jul. 2016.
- [25] Z. Tan, Z. Yan, H. Zhong *et al.*, "Non-iterative solution for coordinated optimal dispatch via equivalent projection – part I: theory," *IEEE Transactions on Power Systems*, vol. 39, no. 1, pp. 890-898, Jan. 2024.
- [26] E. Dall'Anese, S. V. Dhople, and G. B. Giannakis, "Optimal dispatch of photovoltaic inverters in residential distribution systems," *IEEE Transactions on Sustainable Energy*, vol. 5, no. 2, pp. 487-497, Apr. 2014.
- [27] Z. Xu, D. S. Callaway, Z. Hu *et al.*, "Hierarchical coordination of heterogeneous flexible loads," *IEEE Transactions on Power Systems*, vol. 31, no. 6, pp. 4206-4216, Nov. 2016.
- [28] Y. Wen, Z. Hu, S. You *et al.*, "Aggregate feasible region of DERs: Exact formulation and approximate models," *IEEE Transactions on Smart Grid*, vol. 13, no. 6, pp. 4405-4423, Nov. 2022.
- [29] P. Wang, M. Wytoczek, and J. Z. Kolter, "Epigraph projections for fast general convex programming," in *Proceedings of International Conference on Machine Learning*, New York, USA, Jun. 2016, pp. 2868-2877.
- [30] Y. Wen, Z. Hu, and L. Liu, "Aggregate temporally coupled power flexibility of DERs considering distribution system security constraints," *IEEE Transactions on Power Systems*, vol. 38, no. 4, pp. 3884-3896, Jul. 2023.

Rufeng Zhang received the B.S., M.S., and Ph.D. degrees in electrical engi-

neering in Northeast Electric Power University, Jilin, China, in 2013, 2016, and 2019, respectively. He is currently a Professor with the Department of Electrical Engineering of Northeast Electric Power University. His research interests include integrated energy system, power system operation and optimization, and renewable energy integration.

Haodong Liu received the B.S. degree in electrical engineering from Shandong University of Technology, Zibo, China, in 2023, and he is currently working toward the M.S. degree in electrical engineering from Northeast Electric Power University, Jilin, China. His research interests include collaborative active and reactive power optimization, and optimal operation of distribution network and microgrid.

Lizhong Lu received the M.S. degree in agricultural engineering from Shenyang Agricultural University, Shenyang, China, in 2007. He is the Deputy General Manager of State Grid Jilin Power Supply Company, Jilin, China. His research interests include grid coordination optimization, power system operation and planning, and optimization theory and its application.

Yunjing Liu received the M.S. degree in electrical engineering from Northeast Electric Power University, Jilin, China, in 2015. She is the Director of the Party Building Department of State Grid Jilin Power Supply Company, Jilin, China. Her research interests include power quality optimization and improvement of distribution network, and power system operation and optimization.

Linbo Fu received the M.S. degrees in electrical engineering from Northeast Electric Power University, Jilin, China, in 2018. She is currently pursuing the Ph.D. degree in Northeast Electric Power University. Her research interests include energy management of microgrids and operation of distribution market.

Xiaozhuo Guan received the B.S. degree in software engineering from Beijing Institute of Technology, Beijing, China, in 2012. He is the special responsibility of the Science and Technology Department of State Grid Jilin Power Supply Company, Jilin, China. His research interests include energy storage and power system operation and optimization.